Journal of Biomechanics 41 (2008) 656–667

JOURNAL OF BIOMECHANICS

www.elsevier.com/locate/jbiomech
www.JBiomech.com

Bipedal walking and running with spring-like biarticular muscles

Fumiya Iida[a,b,*], Jürgen Rummel[c], André Seyfarth[c]

[a]Computer Science and Artificial Intelligence Laboratory, Massachusetts Institute of Technology, 32 Vassar Street, Cambridge, MA 02139, USA
[b]Artificial Intelligence Laboratory, Department of Informatics, University of Zurich, Andreasstrasse 15, CH-8057 Zurich, Switzerland
[c]Locomotion Laboratory, Institute of Sport Science, University of Jena Dornburger Strasse 23, 07743 Jena, Germany

Accepted 25 September 2007

Abstract

Compliant elements in the leg musculoskeletal system appear to be important not only for running but also for walking in human locomotion as shown in the energetics and kinematics studies of spring-mass model. While the spring-mass model assumes a whole leg as a linear spring, it is still not clear how the compliant elements of muscle–tendon systems behave in a human-like segmented leg structure. This study presents a minimalistic model of compliant leg structure that exploits dynamics of biarticular tension springs. In the proposed bipedal model, each leg consists of three leg segments with passive knee and ankle joints that are constrained by four linear tension springs. We found that biarticular arrangements of the springs that correspond to rectus femoris, biceps femoris and gastrocnemius in human legs provide self-stabilizing characteristics for both walking and running gaits. Through the experiments in simulation and a real-world robotic platform, we show how behavioral characteristics of the proposed model agree with basic patterns of human locomotion including joint kinematics and ground reaction force, which could not be explained in the previous models.

Keywords: Bipedal walking and running; Compliant leg; Biarticular springs; Stability; Legged robot

1. Introduction

The model of ballistic walking was proposed a few decades ago inspired from the observation of relatively low muscle activities during the swing leg of human walking (Mochon and McMahon, 1980). Since then, there have been a number of studies investigating minimalistic walking models (McGeer, 1990; Garcia et al., 1998; Collins et al., 2001), and they inspired for the construction and demonstrations of robotic platforms (Collins et al., 2005).

Although stiff legs are generally assumed in these models, a number of biomechanics studies of human locomotion reported the roles of compliant elements in animals' leg structures (Cavagna et al., 1977; Alexander, 1997; Full and Koditschek, 1999; Dickinson et al., 2000; Srinivasan and Ruina, 2006). Among other results, a recent important discovery is that a theoretical model, the so-called spring-mass model, explains not only the dynamics of human running (Blickhan, 1989; McMahon and Cheng, 1990; Farley and González, 1996; Seyfarth et al., 2002), but also that of walking (Geyer et al., 2006). The importance of this research progress on the compliant leg models lies in the fact that, on the one hand, the dynamics of human walking can be better explained (see the next section for more details), and on the other, a single biped model can explain both walking and running gaits.

While the spring-mass model generally assumes a whole leg as a linear spring, it is still not clear how the elastic components of muscle–tendon systems behave in a human-like segmented leg structure. This study presents a minimalistic model of compliant leg structure that exploits dynamics of biarticular tension springs. In the proposed bipedal model, each leg consists of three leg segments with

*Corresponding author. Tel.: +1 617 324 9136; fax: +1 617 253 0778.
E-mail addresses: iida@csail.mit.edu (F. Iida), andre.seyfarth@uni-jena.de (J. Rummel), juergen.rummel@uni-jena.de (A. Seyfarth).

0021-9290/$ - see front matter © 2007 Elsevier Ltd. All rights reserved.
doi:10.1016/j.jbiomech.2007.09.033

passive knee and ankle joints that are constrained by four linear tension springs. Biarticular arrangements of the springs provide both self-stabilizing and energy efficient characteristics for both walking and running gaits. In particular, we focus on three biarticular tension springs, corresponding to rectus femoris (RF), biceps femoris (BF) and gastrocnemius (GAS) in human legs that play significant roles in the stability and segmental organization of both gaits. The model is analyzed in simulation and in a real-world robotic platform, and we compare the behavior with that of human locomotion.

2. Walking and running in human locomotion

In order to characterize the nature of human walking and running, we first analyze the joint trajectories and ground reaction force (GRF). Hereto, the subject was asked to walk and run on a treadmill operated at a constant velocity of 2 m/s. The locomotion patterns were recorded by motion capture system (six Qualisys motion capture units; sampling frequency of 240 Hz) and two force plates measuring the GRF at each foot. We used 27 tracking points attached to the human subject, from which

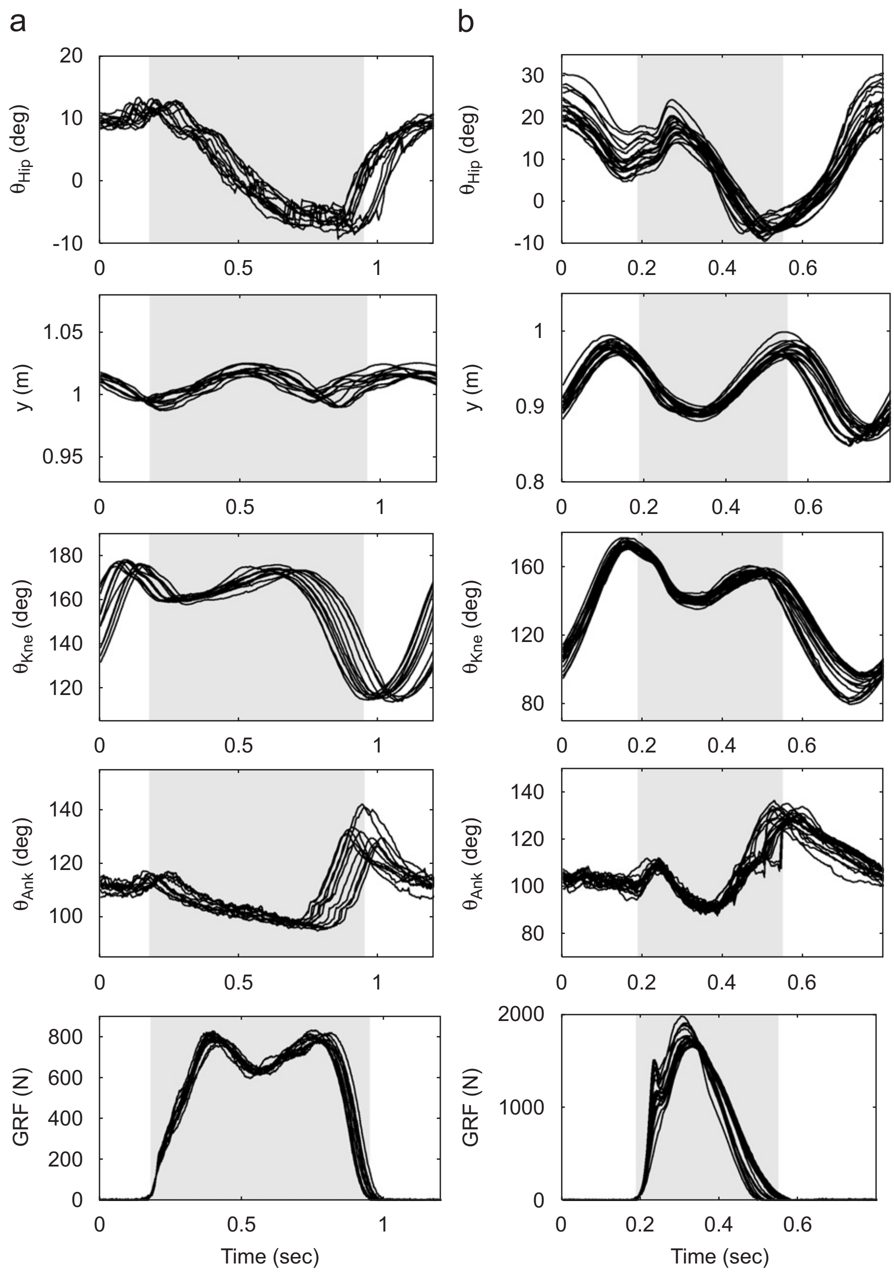

Fig. 1. Time-series trajectories of human locomotion: (a) walking and (b) running both at 2 m/s. The trajectories indicate hip joint angle (θ_{Hip}), vertical movement of body (y), knee joint angle (θ_{Kne}), ankle joint angle (θ_{Ank}) and vertical GRF (from top to bottom figures) of 15 steps which are aligned by the stance phase. The stance phase is indicated by gray rectangle areas in the figures. The coordinate system of the measurement follows the definition in Fig. 2(a).

five points are used to analyze angular movements of the hip, knee and ankle joints. Fig. 1 shows the joint trajectories and vertical GRF of walking and running during 15 steps which are aligned with respect to the stance phase.

A set of basic characteristics of human gaits are shown in these figures, which are generally agreed in biomechanics. Firstly, walking and running dynamics can be clearly distinguished by observing the vertical GRF: while the vertical GRF exhibits two peaks in a stance phase during walking, there is only one peak in running (Keller et al., 1996). Secondly, the vertical body excursion during walking increases toward the middle of the stance phase, whereas it decreases in running (Pandy, 2003; Geyer et al., 2006). And thirdly, in walking, the knee and ankle joints of the stance leg show flexion (Saunders et al., 1953; McMahon, 1984). It is important to note that the ballistic walking models are generally not capable of reproducing some of these aspects of human walking dynamics. For example, the fixed knee joint in the stance leg cannot generate dynamic angular movement (Lee and Farley, 1998), and accordingly, the vertical GRF generally exhibits only one peak in ballistic walking (Pandy, 2003).

Based on these basic observations of human locomotion, in the following sections, we investigate a bipedal locomotion model that generates both walking and running dynamics. To account for the discrepancy between human locomotion and the existing models, we implement the following dynamic elements to the model. Firstly, we employ a simple sinusoidal oscillation in the control of hip joint. Secondly, instead of fixating the passive knee and ankle joints during stance phase as in the ballistic walking model, we constrain the joints by linear tension springs. By having the compliant stance legs, the system is able to reduce ground impact force at touchdown, on the one hand, and to increase the locomotion stability against the irregularity in the foot–ground interaction. And finally, we constrain the movements of the trunk to the horizontal and vertical directions only in order to avoid the complexity derived from the rotational movements.

3. Bipedal locomotion model with compliant legs

The bipedal model investigated in this study consists of seven limb segments (three segments in each leg and one body segment), two motors at the hip joints, four passive knee and ankle joints and eight linear tension springs (Fig. 2). Two ground contact points are defined in each foot segment.

The configuration of springs are determined such that they can constrain the passive joints for natural locomotion behavior, and support the body weight of the entire system. In each leg, three springs are connected over two joints (i.e. two springs attached between the hip and the shank and one between the thigh and the heel). These springs correspond to biarticular muscles, rectus femoris (RF: hip joint flexor and knee joint extensor), biceps femoris (BF: hip joint extensor and knee joint flexor) and

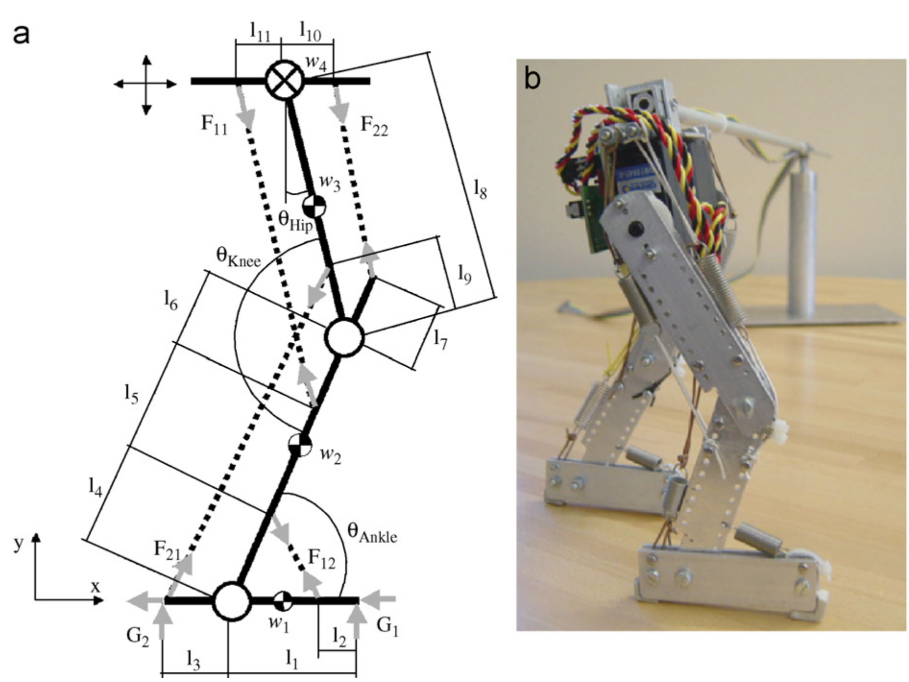

Fig. 2. (a) Bipedal locomotion model with compliant legs (only one of the two legs is shown in this figure). The model consists of an actuated hip joint (denoted by a circle with a cross) and three limb segments which are connected through two passive hinge joints (open circles). The segment mass is defined at the center of each segment. The dashed lines represent the tension springs (S_{11}: BF, S_{12}: TA, S_{21}: GAS and S_{22}: RF), and two ground contact points are defined in the foot segment (G_1 and G_2). The design parameters used in this study are specified in Appendix A. (b) Photograph of the biped robot. Each leg of this robot consists of a hip joint controlled by a servomotor and three leg segments which are connected through two passive joints. Four tension springs are attached to the segments and rubber materials are implemented at the two ground contact points of the foot segment.

gastrocnemius (GAS: knee joint flexor and ankle joint extensor) in human legs. Additionally, a monoarticular spring, corresponding to the tibialis anterior (TA: ankle joint flexor), is implemented. The model parameters are described as $\mathbf{M} = [\mathbf{L}\ \ \mathbf{W}\ \ \mathbf{S}]$, which consists of the individual segment lengths $\mathbf{L} = [l_1 \ldots l_{11}]$, and weight parameters $\mathbf{W} = [w_1\ \ w_2\ \ w_3\ \ w_4]$. As shown in Appendix A, we set the relative proportion of these segment length and weight parameters as close as those of humans while considering the mechanical constraints for robotic implementation such as spring attachment. Three parameters are then used to characterize each spring (spring constant K_{ij}, intrinsic damping factor D_{ij} and rest length N_{ij}) as follows:

$$\mathbf{S} = [\mathbf{S}_{11}\ \ \mathbf{S}_{12}\ \ \mathbf{S}_{21}\ \ \mathbf{S}_{22}] = \begin{bmatrix} K_{11} & K_{12} & K_{21} & K_{22} \\ D_{11} & D_{12} & D_{21} & D_{22} \\ N_{11} & N_{12} & N_{21} & N_{22} \end{bmatrix}. \tag{1}$$

These springs S_{11}, S_{12}, S_{21} and S_{22} correspond to BF, TA, GAS and RF, respectively (Fig. 2). The force generated in these tension springs $\mathbf{F} = [F_{11}\ \ F_{12}\ \ F_{21}\ \ F_{22}]$ are calculated as

$$F_{ij} = \begin{cases} K_{ij}(x_{ij} - N_{ij}) - D_{ij}\dot{x}_{ij}, & x_{ij} > N_{ij}, \\ 0 & \text{otherwise,} \end{cases} \tag{2}$$

where x_{ij} denotes the length of the spring S_{ij}.

This model requires only three control parameters in hip joint actuation: $\mathbf{C} = [A\ \ B\ \ \omega]$, amplitude, offset angle and frequency, respectively. These parameters determine a simple oscillation of the hip joints as follows:

$$\theta_{\mathrm{HipR}}(t) = A \sin(2\pi\omega t) + B, \tag{3}$$

$$\theta_{\mathrm{HipL}}(t) = A \sin(2\pi\omega t + \pi) + B. \tag{4}$$

While the leg segmentation is similar to that of humans, the size of this model is scaled down as shown in Appendix A in order to facilitate the real-world implementation to the robotic platform. And for the sake of simplicity, this model is restricted to motions within a plane, thus no rotational movement (roll or pitch) of the body segment is considered. In the following simulation and robot experiments, all of the parameters $\mathbf{S}$ and $\mathbf{C}$ were determined by considering the geometric constraints explained in Section 5.

For the simulation experiments, we implemented the model to Matlab (The Mathworks Inc.) together with the SimMechanics toolbox. A level ground surface with a physically realistic interaction model is defined based on Gerritsen et al. (1995). The vertical GRFs are approximated by nonlinear spring–damper interaction, and the horizontal forces are calculated by a sliding–stiction model. The model switches between sliding and stiction when the velocity of the foot becomes lower or higher than the specified limit determined by the sliding and stiction friction coefficients, μ_{slide} and μ_{stick}, respectively.

$$G_{yi} = a|y_{ci}|^3(1 - b\dot{y}_{ci}), \tag{5}$$

$$G_{xi} = \begin{cases} \mu_{\mathrm{slide}} G_{yi} \dfrac{\dot{x}_{ci}}{|\dot{x}_{ci}|} & \text{if } F_{xci} > \mu_{\mathrm{stick}} G_{yi} \dfrac{\dot{x}_{ci}}{|\dot{x}_{ci}|}, \\ F_{xci} & \text{otherwise,} \end{cases} \tag{6}$$

where $\dot{x}_{ci}$ and y_{ci} denote the horizontal velocity and the vertical distance of the contact point i from the ground surface, respectively. F_{xci} represents the computed force at the foot contact point i. We used the following parameters to simulate the ground interaction: $a = -2.5 \times 10^5\,\mathrm{N/m^3}$, $b = 3.3\,\mathrm{s/m}$, $\mu_{\mathrm{slide}} = 0.6$ and $\mu_{\mathrm{stick}} = 0.7$.

In parallel, the model was implemented to a robotic platform as shown in Fig. 2(b). This robot consists of passive knee and ankle joints, and two servomotors (Conrad HS-9454) at the hip joints as in the simulation model. We used four tension springs and rubber material at the two ground contact points in each foot segment in order to gain sufficient ground friction and to minimize impact force at touch down. A supporting boom was attached to the body segment in order to restrict roll and pitch of the upper body segment. The same control parameters were used to conduct a set of experiments. Since this robot is not able to change the spring parameters, we tuned the parameters before each experiment.

4. Dynamics of walking and running

The dynamics of the proposed model is analyzed in terms of the time-series data of system variables, vertical body movement (y), knee and ankle joints (θ_{Knee} and θ_{Ankle}), vertical GRF ($G_{y1} + G_{y2}$) and a vector of forces generated in the springs ($\mathbf{F}$). The GRF of one leg is defined as a sum of GRF in two contact points of the foot (Fig. 2).

With the spring and control parameters $\mathbf{S}_{\mathbf{walk}}$ and $\mathbf{C}_{\mathbf{walk}}$ (see Appendix A), the model exhibits stable walking gait as shown in Figs. 3(a) and (c) and 4(a).[1] The behavior of each joint shows the similarity to those of human walking (Fig. 1(a)). More specifically, in Fig. 3(a), the knee joint starts slightly flexing at the beginning of stance phase (0.09 s), extending and flexing again toward the end (0.27 s). The ankle joint extends at the end of stance phase which results in ground clearance for the subsequent swing phase. Note that the spring S_{12} (TA) generates small force during the swing phase which stabilizes the ankle joint at the angle required for ground clearance.

For a running gait, the spring and control parameters are set to $\mathbf{S}_{\mathbf{run}}$ and $\mathbf{C}_{\mathbf{run}}$ in which the spring constants K_{ij} and the motor oscillation frequency ω are set to significantly larger values than those of walking. In addition, the rest length of spring N_{11} (BF) is set to a

[1] See also the video clip of the simulation and robot experiments (Appendix A).

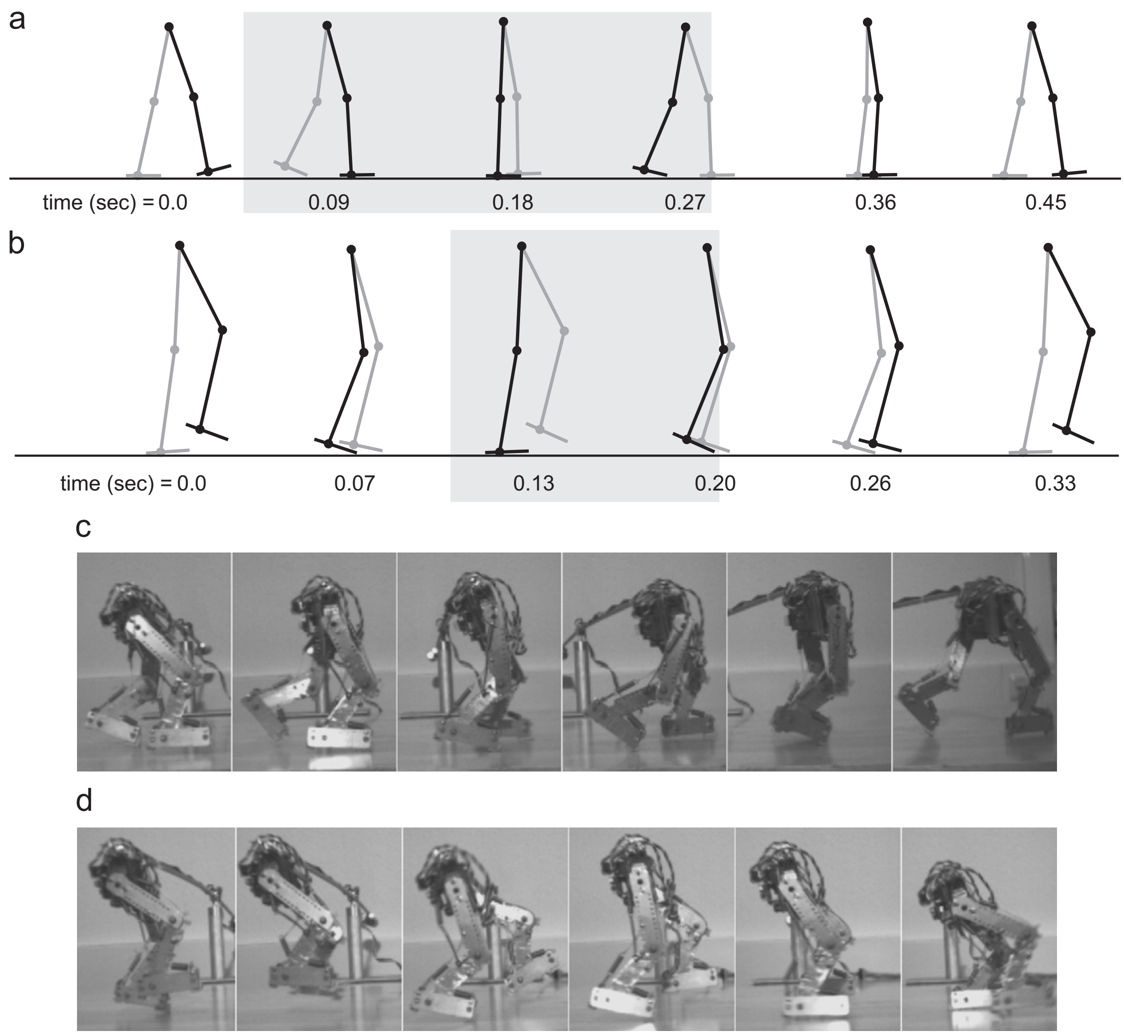

Fig. 3. One cycle behavior of the model in simulation: (a) walking and (b) running. Black and gray leg segments represent the right and left legs, respectively, and gray areas depict the stance phase of the right leg. The cycle time is set to 0.45 s ($\omega = 2.2$ Hz) for walking, and 0.33 s ($\omega = 3.0$ Hz) for running. The flight phase of running is approximately 0.06 s before and after the stance phase (see also Fig. 4(b)). Time-series photographs of the biped robotic platform during (c) walking and (d) running. A high-speed camera was used to record the experiments (Basler A602 fc: resolution 656 × 490 pixels, frame rate 100 fps). The interval between two pictures is approximately 10 ms. See also the video clip in Appendix A.

shorter length for antagonistic torque equilibrium at the knee joint. As shown in Figs. 3(b) and (d) and 4(b), the running gait exhibits clear flight phases (around 0.07 and 0.26 s). By comparing the simulation results with those of human (Figs. 1(b) and 4(b)), the knee and ankle joints show similar behavioral patterns. For example, the knee joint exhibits multiple peaks in a cycle (0.10 and 0.20 s), and the ankle joint flexes and extends in the stance phase.

The contrast between two gaits, that is similar to human locomotion, can be observed in the vertical body excursion and the vertical GRF (Fig. 4). Namely, this model exhibits the maximum peak of vertical body movement in the stance phase in walking (0.12 s in Fig. 4(a)), while the minimum peak in running (0.13 s). In addition, vertical GRF shows multiple humps during walking while there is a large bell curve in running.

The roles of biarticular spring arrangement can be identified further by comparing with the model that has only monoarticular arrangement of the springs by setting $l_{9,10,11} = 0$. With the spring and control parameters $\mathbf{S}^{\mathbf{m}}_{\mathbf{walk}}$, $\mathbf{S}^{\mathbf{m}}_{\mathbf{run}}$, $\mathbf{C}^{\mathbf{m}}_{\mathbf{walk}}$ and $\mathbf{C}^{\mathbf{m}}_{\mathbf{run}}$ (see Appendix A), the model with monoarticular spring arrangement can also perform periodic gait patterns as shown in Fig. 5. By comparing with Fig. 4, however, there are a few salient differences. Firstly, because the hip motor torque and GRF do not directly influence the knee and ankle joints through the springs, the model with monoarticular springs exhibits less joint dynamics especially in running. Namely the knee and ankle joints show significantly smaller fluctuation in both stance and swing phases. Secondly, the monoarticular spring arrangement often induces locomotion instability originated in kinematic singularity of the knee joint (i.e. the joint angle exceeds 180°). For this reason, the knee joint angle needs to be maintained at a relatively lower angle with smaller dynamics, although the biarticular arrangement allows the legs to extend up to 180°.

Fig. 6 shows the kinematics and GRF during 10 steps of the robot walking and running. In general, the

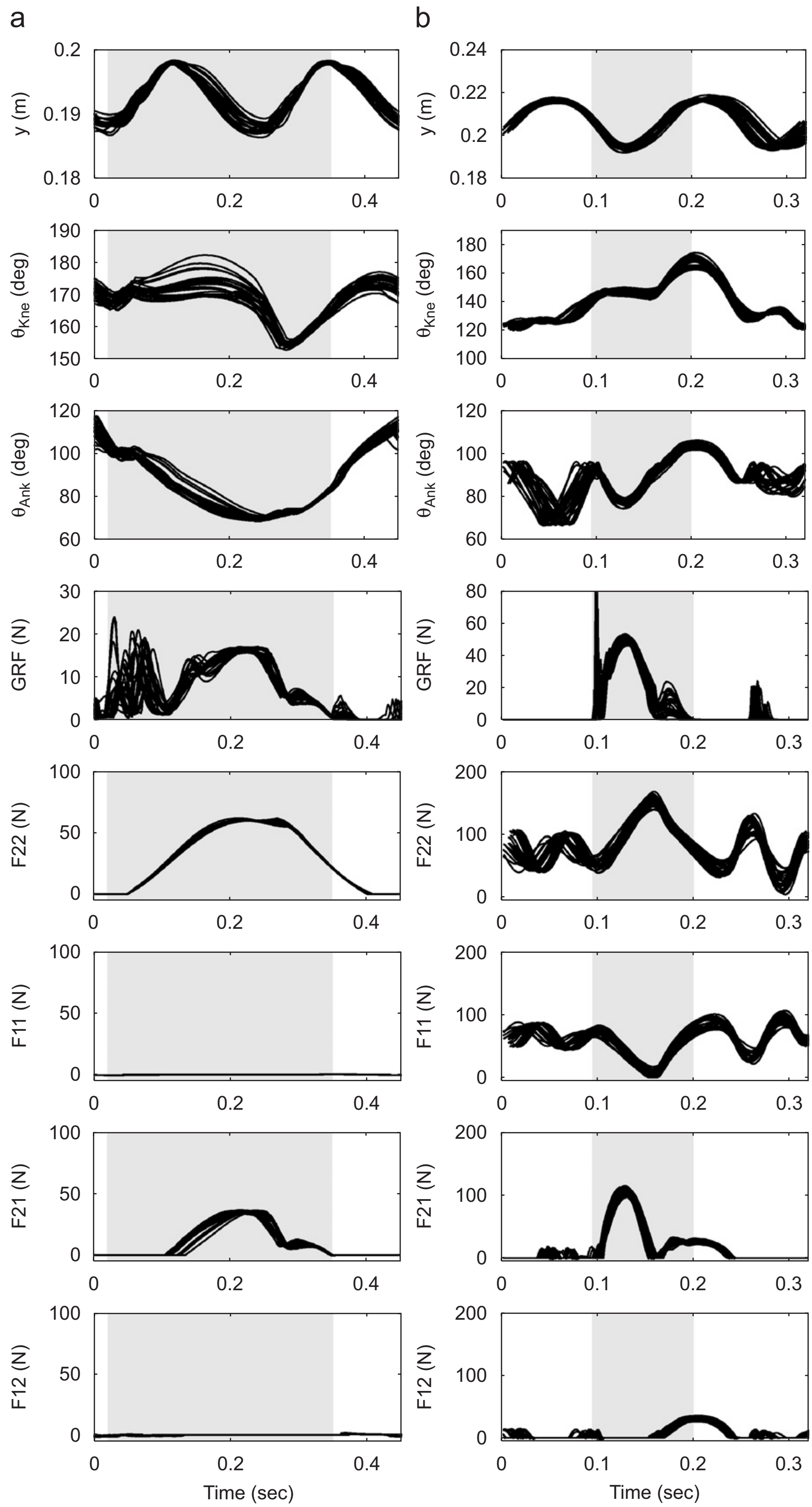

Fig. 4. Time-series trajectories of the model in simulation: (a) walking and (b) running. The trajectories of vertical hip joint movement (indicated by y), angular trajectories of knee (θ_{Kne}) and ankle (θ_{Ank}) joints, vertical GRF and the forces F_{22}, F_{11}, F_{21} and F_{12} generated in springs S_{22} (RF), S_{11} (BF), S_{21} (GAS) and S_{12} (TA), respectively. The experimental data of 20 steps are aligned by the stance phase (indicated by the gray areas in the figure).

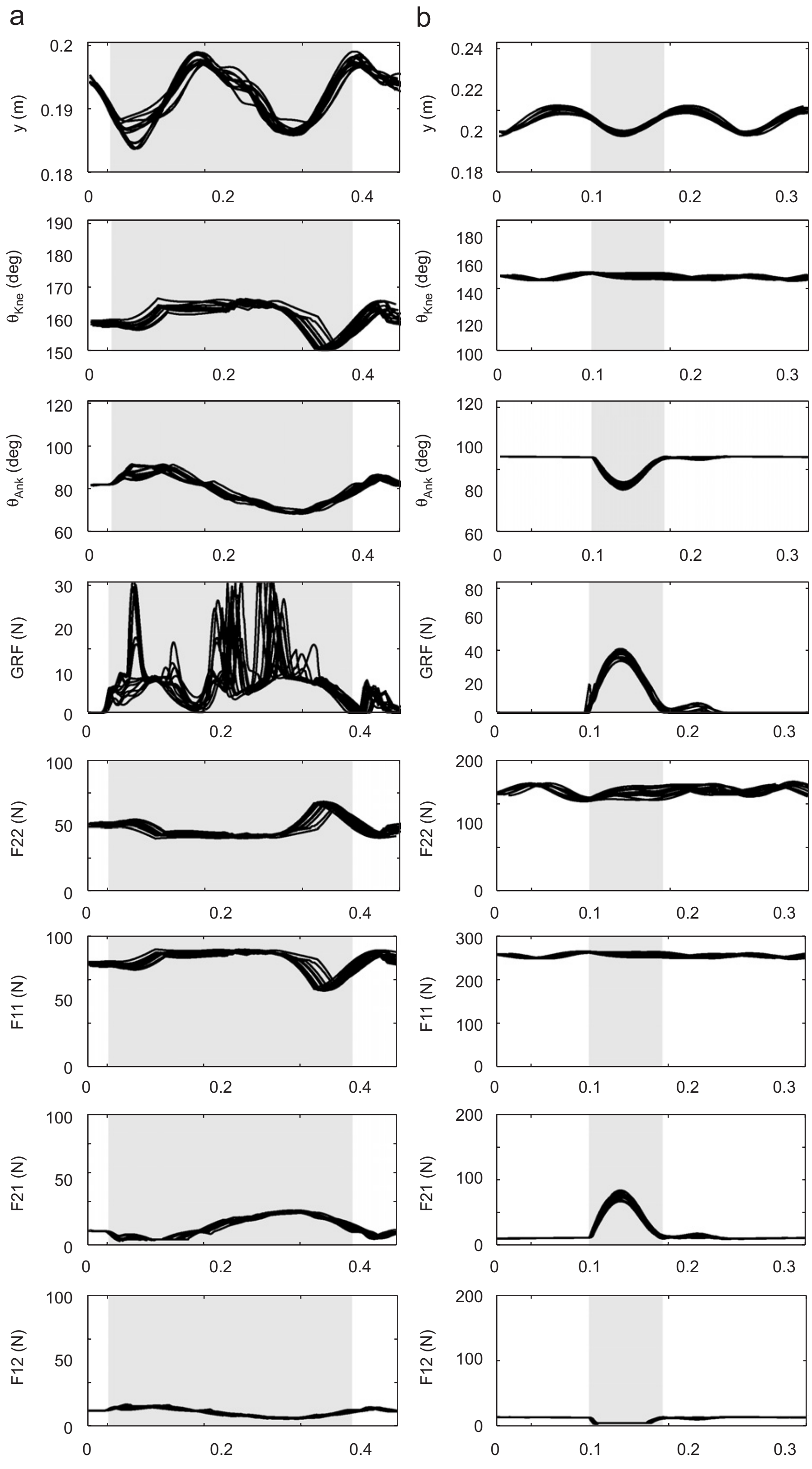

Fig. 5. Simulated behavior of the model with a monoarticular spring arrangement ($l_{9,10,11} = 0$): (a) walking with the parameters $\mathbf{S}^{\mathbf{m}}_{\mathbf{walk}}$ and $\mathbf{C}^{\mathbf{m}}_{\mathbf{walk}}$, and (b) running with $\mathbf{S}^{\mathbf{m}}_{\mathbf{run}}$ and $\mathbf{C}^{\mathbf{m}}_{\mathbf{run}}$. The trajectories of vertical hip joint movement (indicated by y), angular trajectories of knee (θ_{Kne}) and ankle (θ_{Ank}) joints, vertical GRF and the forces F_{22}, F_{11}, F_{21} and F_{12} generated in springs S_{22}, S_{11}, S_{21} and S_{12}, respectively. The experimental data of 20 steps are aligned by the stance phase (indicated by the gray areas in the figure).

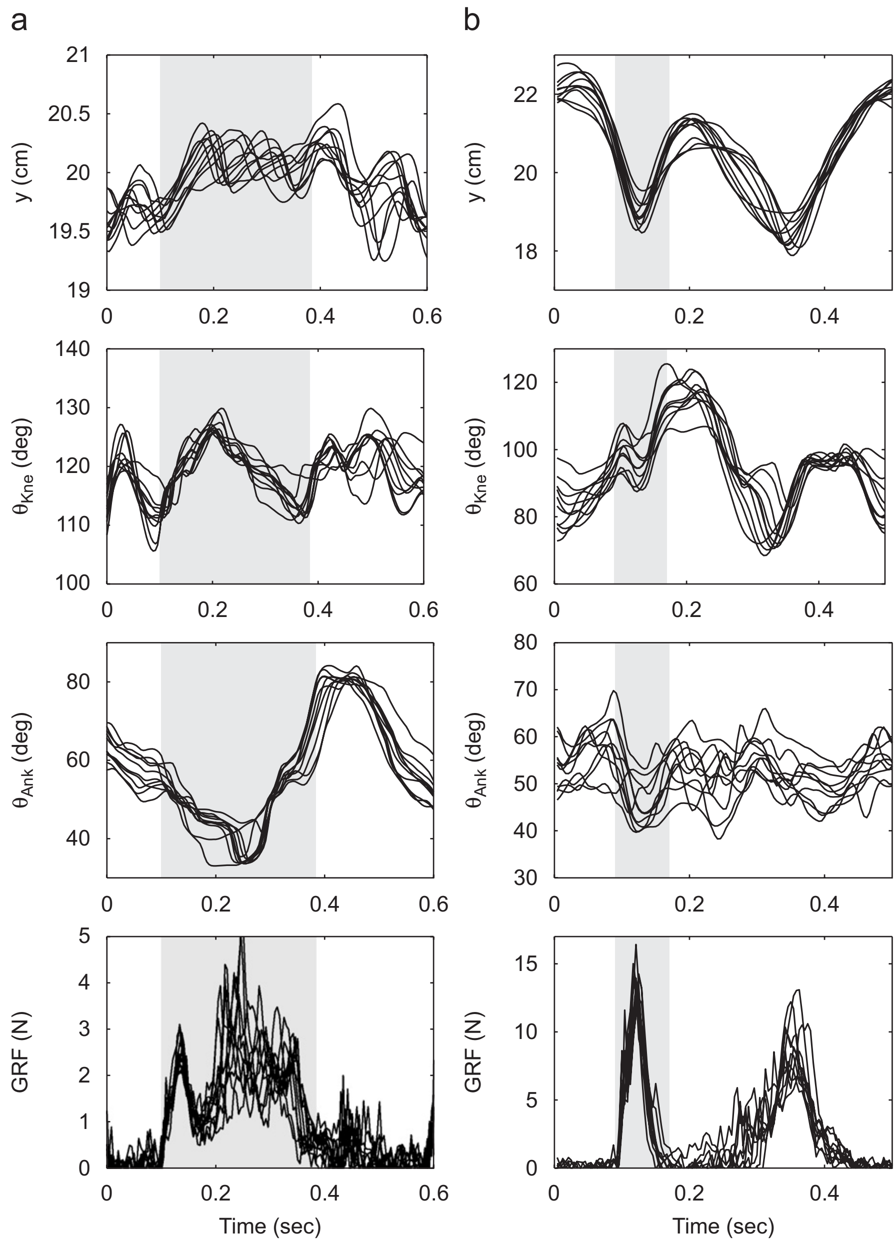

Fig. 6. Time-series trajectories of the robotic platform: (a) walking and (b) running. Vertical movements of body (indicated by y), knee joint angle (θ_{Kne}), ankle joint angle (θ_{Ank}) and vertical GRF (from top to bottom figures) are aligned by the stance phase of 10 steps (the stance phase is indicated by gray rectangle areas in the figures). The data were measured by high-speed infrared cameras for motion capture (Qualisys ProReflex; sampling frequency 240 Hz) and force plates (Kistlerr 9281B11; sampling frequency 1000 Hz). The joint kinematics were extracted from 10 reflective markers attached to the robot. Note that, in the running experiments, both legs of the robot are on the same force plate, thus the second peak of the GRF indicates the force generated by the other leg.

experimental results show a good agreement with the simulation results: the vertical excursion of the body reaches the lowest peak at the stance phase in running, and the highest peak in walking. Moreover, the vertical GRF shows multiple peaks in walking while there is a single peak in running. The trajectories of the knee and ankle joints also show the similarity to those of human locomotion and simulation experiments. In walking, the knee joint angle increases at the middle of stance phase and the ankle joint angle increases toward the end of stance phase. In contrast, during running, the knee joint angle significantly decreases in the middle of swing phase.

5. Self-stabilization of locomotion gaits

The stability of these two gait patterns is based on the underlying system dynamics. Namely, without explicit control of every joint, the basic motor oscillation signals induce the whole body dynamics, with which the system stabilizes itself into the periodic gait cycles over extended period of time. Because the forces of gravity, GRF and hip

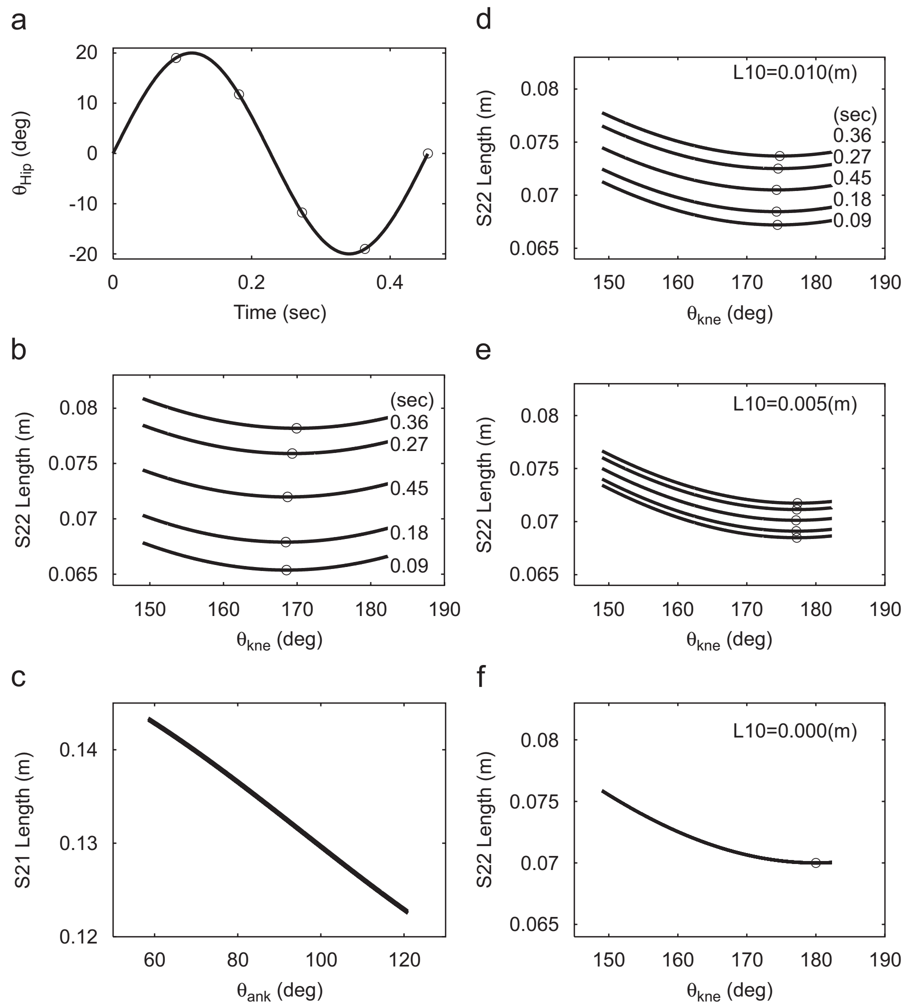

Fig. 7. Geometric constraints of the biarticular springs S_{22} and S_{21} in the proposed model. (a) A single cycle of hip joint trajectory. Circles depict the sampling points that are used to calculate the spring length of S_{22} and S_{21} in (b–f). (b) Changes of the spring length S_{22} with respect to the knee joint angle ($l_{10} = 0.020$ m). Five lines correspond to the sampling points of the hip joint. Circles depict the minimum length of S_{22} in each sampling point, which is used in (c). (c) Changes of the spring length S_{21} with respect to the ankle joint angle. Five lines are mostly overlapped. The cycle time is set to 0.45 s ($\omega = 2.2$ Hz), corresponding to the walking simulation. (d–f) Influence of the parameter l_{10} to the relation between the S_{22} spring length and the knee joint angle θ_{kne} ($l_{10} = 0.010, 0.005, 0.000$ m, respectively). With $l_{10} = 0.000$ m, the spring S_{22} becomes monoarticular arrangement, and five lines follow the same profile.

joint actuation are mediated by the compliant elements of the leg structure, we analyze the behavior of springs during walking and running in this section.

First we analyze the geometric constraints derived from biarticular springs S_{22} (RF) and S_{21} (GAS) which are active during walking (Fig. 4(a)). Fig. 7 shows the geometric constraints of S_{22} and S_{21} with respect to the hip, knee and ankle joint angles. This analysis considers only geometric relation between joint angles, segment and spring length, thus no forces are acted on the limb segments (i.e. spring forces or GRF).

In general, the length of biarticular spring S_{22} becomes larger as the hip joint extends (i.e. the decrease of θ_{Hip} in Fig. 7(a)), which generates the dynamic knee joint trajectories during the stance phase. In addition, toward the end of the swing phase, it becomes smaller (resulting in knee joint protraction) as the hip joint flexes. This is a unique property of the biarticular arrangement as shown in Fig. 7(b) and (d)–(f). With a monoarticular arrangement $l_{10} = 0.000$ m (Fig. 7(f)), for example, the knee joint angle is fixed at 180° regardless of the hip joint angle, and as the l_{10} parameter becomes larger, the knee joint angle depends more on the hip joint angle. Note that, with a given hip joint angle, the length of spring S_{22} has a minimum value with respect to the knee joint (depicted by the open circles in Fig. 7(b)). Given a proper rest length of S_{22}, therefore, the spring generates force that guides the knee angle toward the minimum point of spring length, i.e. the preferred knee angle. The length of biarticular spring S_{21} decreases proportionally with respect to the ankle joint angle (Fig. 7(c)).

Fig. 8 shows how the springs S_{22} and S_{21} follow the geometric constraints during the walking simulation shown in Figs. 3(a) and 4(a). The forces generated by the springs

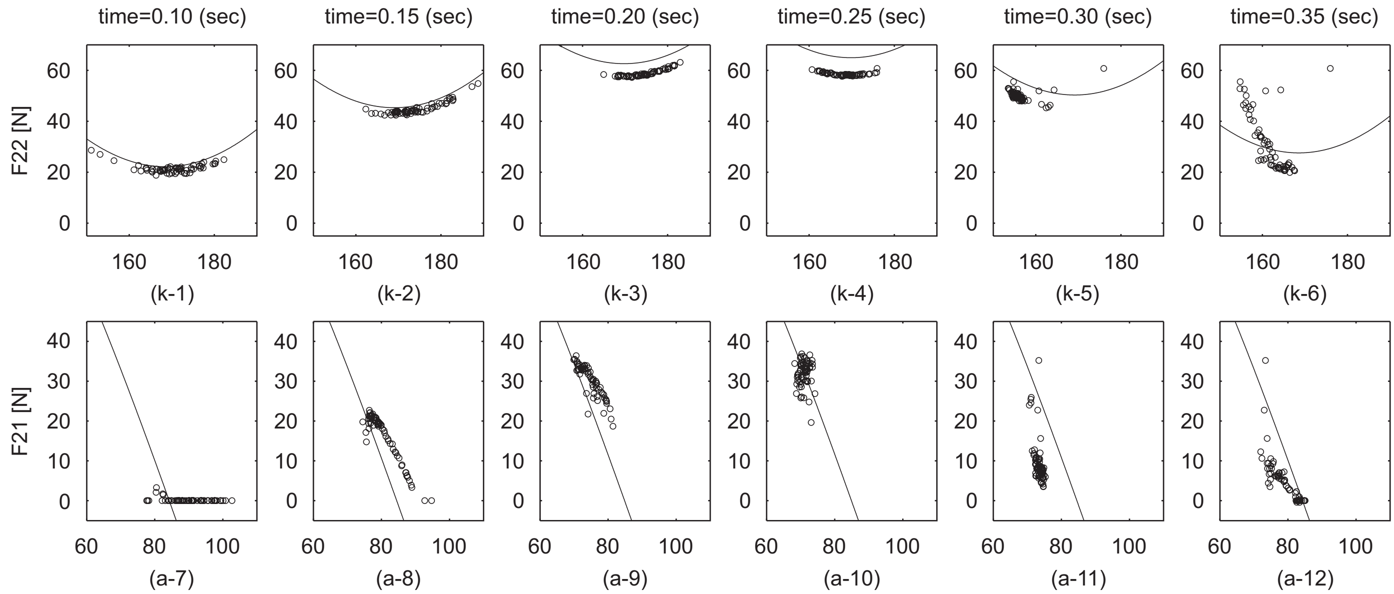

Fig. 8. Force generated at different time steps (0.10−0.35 s) by the springs S_{22} (RF, k-1–6), and S_{21} (GAS, a-7–12) in the walking simulation (corresponding to Figs. 3(a) and 4(a)). The forces are plotted with respect to the knee and ankle joint angles. Lines represent the calculated force profiles translated from Fig. 7(b) by using the hip joint angles, the spring constants and rest length of S_{walk} in Appendix A. The calculated F_{21} profiles assume the minimum values of the calculated knee profiles.

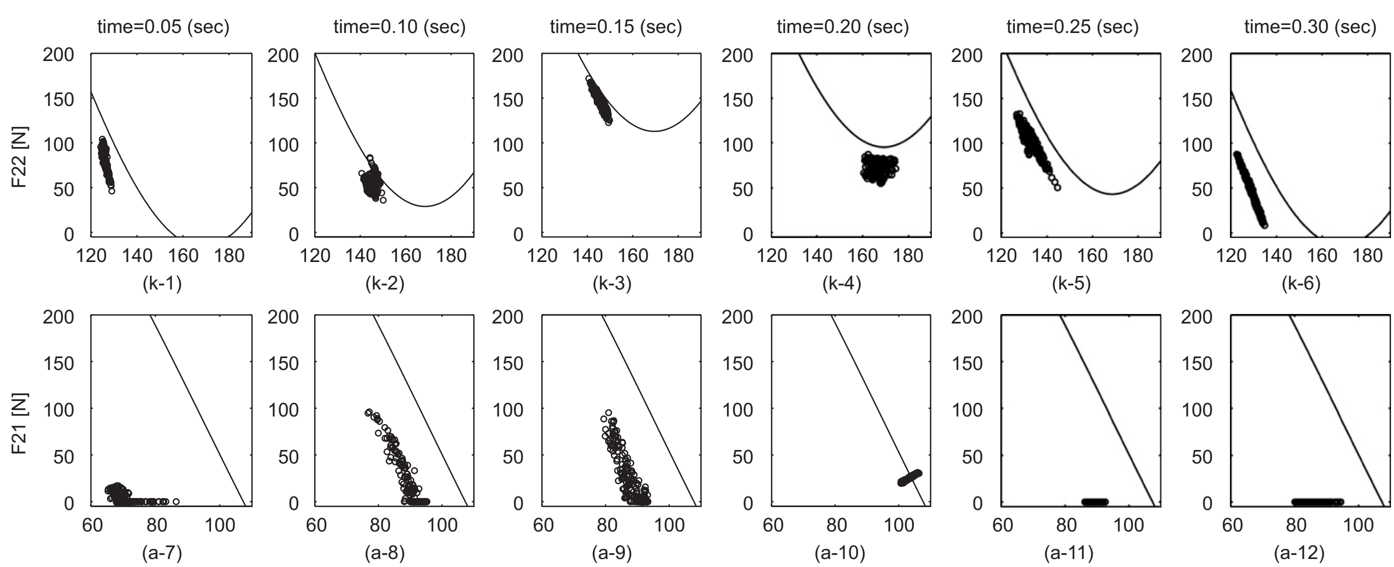

Fig. 9. Force generated by the springs S_{22} (k-1–6), and S_{21} (a-7–12) in the running simulation (corresponding to Figs. 3(b) and 4(b)). The forces are plotted with respect to the knee and ankle joint angles. Lines represent the calculated force profiles translated by using the hip joint angles, the spring constants and rest length of S_{run} in Appendix A.

S_{22} and S_{21} during 20 steps of walking are plotted with respect to knee joint angle. Fig. 8(k-1) to (k-6) shows that, during the most of the period of stance phase (0.05–0.25 s), the knee angles are centered around the preferred angles until the end of stance phase. In addition, Fig. 8(a-7) to (a-12) explains how the spring S_{21} is used to push up the foot off the ground for the swing phase; the spring S_{21} starts generating the force as the leg swings backward (around 0.09 s), and it is deactivated in the swing phase (after 0.30 s).

In contrast to walking, the springs S_{22} and S_{21} behave differently in running. Fig. 9 shows that the distribution of the force generated by the spring S_{22} is clearly shifted from the preferred angle of knee joint (around 170°). Because the spring S_{11} (BF) generates force as well as S_{22} (see Fig. 4(b)), the knee angle is shifted from the preferred angle particularly at the beginning of stance phase (up to 0.15 s). As the leg swings backward (0.20 s), the spring S_{11} decreases its tension force, which results in a stretch of

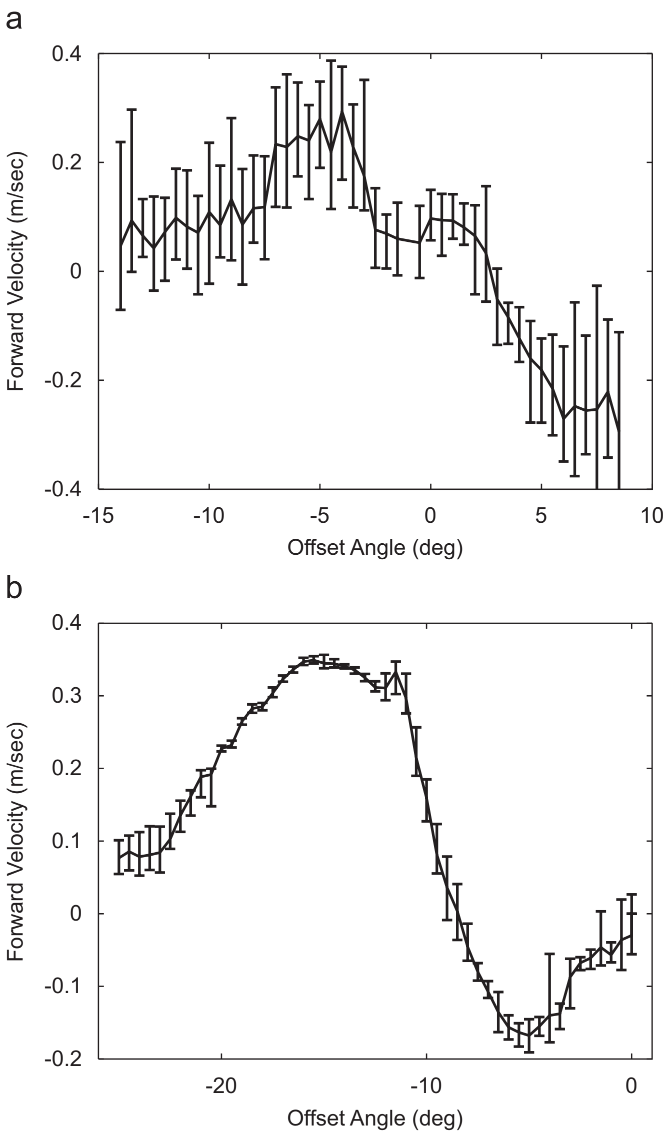

Fig. 10. Forward velocity of (a) walking and (b) running behavior in simulation with respect to the offset angle B of the motor oscillation (Eqs. (3) and (4)). The mean forward velocity (solid line) during a 10-s experiment was measured in 10 different coefficients of ground friction ($0.65 < \mu_{stick} < 0.85$ and $0.45 < \mu_{slide} < 0.65$). The vertical error bars represent the variance induced by the different ground friction.

the knee joint for the takeoff of the leg. Note that the spring S_{21} also contributes significantly to the takeoff of the leg (between 0.10 and 0.15 s).

From this analysis, it can be concluded that the walking and running gaits are generated through two different stabilization mechanisms in this model. In walking, stability of knee joint is maintained primarily by the basin of attraction derived from the geometric constraint of the spring S_{22}. In contrast, during running, the equilibrium of the knee joint angle is determined by the two antagonistic springs S_{22} and S_{21}.

These two mechanisms for the different gaits can be characterized further by varying the motor control parameters. Fig. 10 shows the forward velocity of walking and running in different offset angles of motor oscillation and the coefficients of ground friction. This analysis shows that the walking and running gaits of this model can be used for various forward locomotion velocities. In addition, although the maximum velocities are not significantly different between walking and running (approximately 0.35 m/s), the running gait is more stable than walking one considering the smaller variance against different ground friction. It is important to note that the similar changes of forward velocity can be observed by using the other parameters of amplitude and frequency (i.e. A and ω in Eqs. (3) and (4)). These motor parameters are the potential variables for controlling the forward locomotion velocity.

6. Discussion and conclusion

This study presented a minimalistic bipedal locomotion model with compliant legs that utilize biarticular arrangement of tension springs. With experiments in simulation and in the real-world robotic platform, we showed that this model provides two eminent features that could not be explained by the other simple models such as the ballistic walking. Firstly, the compliant elements in the leg structure make the model possible to generate both walking and running gaits. And secondly, owing to the biarticular arrangements of the tension springs, this model is able to achieve more human-like leg movements compared with those of ballistic walking.

In the segmented leg structure, compliant elements can also be modelled at joint level by utilizing monoarticular springs as shown in Kuitunen et al. (2002), Günther and Blickhan (2002) and Pratt (2002), for example. The present study, however, showed the potential roles of biarticular muscle arrangements, RF, BF and GAS (corresponding to S_{22}, S_{11} and S_{21}, respectively). From the experimental results, it can be concluded that biarticular muscles do support energy transfer between the joints for the self-stabilization of walking and running gaits. Note that TA (S_{12}) is mainly lifting the foot in swing phase.

The results of this study also demonstrated that a simple oscillation at the actuated hip joints is sufficient to generate both walking and running gaits without sensory feedback, if the leg compliance is properly tuned. In the spring-mass model, for example, it is not explicitly discussed how to control the touchdown angle of legs, which is one of the critical parameters with respect to the stability of periodic stable locomotion (Blickhan, 1989; McMahon and Cheng, 1990; Seyfarth et al., 2002). From the demonstrations of bipedal walking and running in this study, it could be concluded that the touchdown angles of the legs can be achieved with no explicit feedback control but by self-organization of the system dynamics.

Although the human-like locomotion dynamics of the proposed model was observed mainly in vertical excursion of the body and dynamic trajectories of the knee and ankle joints during stance phase, the proposed model was not designed to fully explain the dynamics of human walking and running. For example, the walking gait exhibited only modest ground clearance during swing phase, resulting in a large deviation of vertical GRF at the beginning of stance phase (Fig. 4(a)). Furthermore, the running gait analyzed in this study was more similar to jogging at slow velocity or hopping at place in human locomotion (i.e. the touchdown angle of stance leg is smaller than that of swing leg as shown in Fig. 3(b)). These results imply the limit of the proposed model.

Conflict of interest

All of the sponsors are indicated in the acknowledgment and there is no conflict of interest that could inappropriately influence our work.

Acknowledgments

This work is supported by the German Research Foundation (DFG, SE1042), the Swiss National Science Foundation (Grant no. 200021-109210/1) and the Swiss National Science Foundation Fellowship for Prospective Researchers (Grant no. PBZH2-114461). The authors would like to appreciate Susanne Lipfert and our other collaborators for providing us the experimental results of human locomotion.

Appendix A. Supplementary data

Supplementary data associated with this article can be found in online version at doi:10.1016/j.jbiomech.2007.09.033.

References

Alexander, R.McN., 1997. A model of bipedal locomotion on compliant legs. Philosophical Transactions of the Royal Society of London Series B 338, 189–198.

Blickhan, R., 1989. The spring-mass model for running and hopping. Journal of Biomechanics 22, 1217–1227.

Cavagna, G., Heglund, N., Taylor, C., 1977. Mechanical work in terrestrial locomotion: two basic mechanisms for minimizing energy expenditure. American Journal of Physiology 233, 243–261.

Collins, S., Ruina, A., Tedrake, R., Wisse, M., 2005. Efficient bipedal robots based on passive dynamic walkers. Science 307, 1082–1085.

Collins, S.H., Wisse, M., Ruina, A., 2001. A three-dimensional passive-dynamic walking robot with two legs and knees. International Journal of Robotics Research 20, 607–615.

Dickinson, M., Farley, C., Full, R., Koehl, M., Kram, R., Lehman, S., 2000. How animals move: an integrative view. Science 288, 100–106.

Farley, C., González, O., 1996. Leg stiffness and stride frequency in human running. Journal of Biomechanics 29 (2), 181–186.

Full, R., Koditschek, D., 1999. Templates and anchors: neuromechanical hypotheses of legged locomotion on land. Journal of Experimental Biology 202, 3325–3332.

Garcia, M., Ruina, A., Chatterjee, A., Coleman, M., 1998. The simplest walking model: stability, complexity, and scaling. Journal of Biomechanical Engineering 120 (2), 281–288.

Gerritsen, K.G.M., van den Bogert, A.J., Nigg, B.M., 1995. Direct dynamics simulation of the impact phase in heel-toe running. Journal of Biomechanics 28 (6), 661–668.

Geyer, H., Seyfarth, A., Blickhan, R., 2006. Compliant leg behaviour explains basic dynamics of walking and running. Proceedings of Royal Society of London Series B 273, 1471–2954.

Günther, M., Blickhan, R., 2002. Joint stiffness of the ankle and the knee in running. Journal of Biomechanics 35 (11), 1459–1574.

Keller, T.S., Weisberger, A.M., Ray, J.L., Hasan, S.S., Shiavi, R.G., Spengler, D.M., 1996. Relationship between vertical ground reaction force and speed during walking, slow jogging, and running. Clinical Biomechanics 11 (5), 253–259.

Kuitunen, S., Komi, P., Kyrolainen, H., 2002. Knee and ankle joint stiffness in sprint running. Medicine and Science in Sports and Exercise 34 (1), 166–173.

Lee, C., Farley, C., 1998. Determinants of the center of mass trajectory in human walking and running. Journal of Experimental Biology 201, 2935–2944.

McGeer, T., 1990. Passive dynamic walking. International Journal of Robotics Research 9 (2), 62–82.

McMahon, T.A., 1984. Muscles, Reflexes, and Locomotion. Princeton University Press, Princeton, NJ.

McMahon, T.A., Cheng, G.C., 1990. The mechanics of running: how does stiffness couple with speed? Journal of Biomechanics 23 (1), 65–78.

Mochon, S., McMahon, T.A., 1980. Ballistic walking. Journal of Biomechanics 13, 49–57.

Pandy, M.G., 2003. Simple and complex models for studying muscle function in walking. Philosophical Transactions of the Royal Society of London Series B 358, 1501–1509.

Pratt, G.A., 2002. Low impedance walking robots. Integrative and Comparative Biology 42 (1), 174–181.

Saunders, J.B., Inman, V.T., Eberhart, H.D., 1953. The major determinants in normal and pathological gait. Journal of Bone and Joint Surgery 35A, 543–558.

Seyfarth, A., Geyer, H., Guenther, M., Blickhan, R., 2002. A movement criterion for running. Journal of Biomechanics 35, 649–655.

Srinivasan, M., Ruina, A., 2006. Computer optimization of a minimal biped model discovers walking and running. Nature 439 (5), 72–75.